ELSEVIER

Contents lists available at ScienceDirect

Journal of Hydrology

journal homepage: www.elsevier.com/locate/jhydrol



Research papers

Divergent patterns of rainfall regimes in dry and humid areas of China

Ying Hu^{a,b}, Fangli Wei^c, Bojie Fu^{a,b,*}, Shuai Wang^d, Xiangming Xiao^e, Yuanwei Qin^e, Shihua Yin^a, Zhuangzhuang Wang^a, Lingfan Wan^{a,b}

- a State Key Laboratory of Urban and Regional Ecology, Research Center for Eco-Environmental Sciences, Chinese Academy of Sciences, Beijing 100085, China
- ^b University of Chinese Academy of Sciences, Beijing 100049, China
- ^c Key Laboratory of Ecosystem Network Observation and Modeling, Institute of Geographic Sciences and Natural Resources Research, Chinese Academy of Sciences, Beijing 100101, China
- d State Key Laboratory of Earth Surface Processes and Resource Ecology, Faculty of Geographical Science, Beijing Normal University, Beijing 100875, China
- e Department of Microbiology and Plant Biology, School of Biological Sciences, University of Oklahoma, Norman, OK, USA

ARTICLE INFO

Keywords: Wet season Dry spell Onset Cessation Climate risks

ABSTRACT

Monitoring the long-term dynamics of the wet season is important for both the current operation and future management of water resource systems. Wet seasons in China are substantially influenced by monsoons with great variability but are unknown. We conducted a comprehensive assessment of rainfall regimes in China between 1982 and 2020 using a modified anomalous accumulation method at the pixel level. We observed divergent patterns of "wet areas becoming drier, and dry areas becoming wetter" with rainfall amount and rainy days increasing in dry regions, and decreasing in humid regions. Wet seasons extend to dry areas and shorten in wet areas, with trends related to dryness. Simultaneously, as the dryness increased, the length, number of dry spells, and consecutive dry days increased. Concurrent increases in rainy days and dry spells indicated a seasonal rainfall regime toward greater variations in drier areas, which was not entirely consistent with a global intensification pattern of "dry getting drier and wet getting wetter", implying increased potential climatic risks in dry areas. For climate risk prediction, water resource allocation, and agricultural management, we advocate a finer and more precise dynamic assessment of the wetting—drying pattern.

1. Introduction

The wet season refers to the period of the year when the majority of annual precipitation occurs in a certain region or country, and is one of the basic necessities of research on climate change, drought, and flood disasters (Funk et al., 2019; Zhou et al., 2022a). China, which is located at the mid-latitudes, is influenced by the Asian monsoon (Guo et al., 2020). Rainfall shows distinct intra-annual distribution differences and is highly concentrated during the wet seasons (Dai et al., 2020). Wet seasons in China have gained a considerable attention from the academic community, as their variations are linked to hydrological cycles and the Asian monsoon, which is an important component of global atmospheric circulation and substantially affects crop production and social security (Zhang et al., 2018; Zhou et al., 2022a; Zhang et al., 2023).

However, inconsistent definitions of wet seasons have resulted in a limited number of studies on rainfall regimes (Kniveton et al., 2009;

Seregina et al., 2019). Most studies on the onset and cessation of the wet season in China have used a qualitative method on a regional scale, which is relatively arbitrary; for example, Meiyu from June to August over the middle and lower reaches of the Yangtze River, (Ge et al., 2008) autumn wet season in Western China (Zhang et al., 2019a), summer monsoon rainfall in Southeast China (Dai et al., 2020), and three-stage summer precipitation during early summer, Meiyu season, and late summer (Liu et al., 2020). Quantitatively, rainfall amount is the basic criterion. For example, Wang (2020) defined Asian wet seasons by relative climatic pentad rainfall, and Wu (2024) conducted a comparative analysis of different pentad precipitation to determine the onset and end of the wet season in Southwest China. However, it is difficult to accurately reflect the characteristics of the wet season in China because of different rainfall amounts in different subareas, as well as diverse terrain features and monsoon systems (Guo et al., 2022). In this context, a unified study of the wet season in China is required with finer descriptions at different places.

E-mail address: bfu@rcees.ac.cn (B. Fu).

^{*} Corresponding author at: at: State Key Laboratory of Urban and Regional Ecology, Research Center for Eco-Environmental Sciences, Chinese Academy of Sciences, Beijing 100085, China.

Intensified hydrological cycles under global warming further increase uncertainties in wet season variations in China (Guo et al., 2020; Ferijal et al., 2021). Extensive research has been conducted to investigate alterations in precipitation around totals (including mean values) and tails (i.e. extreme precipitation based on a certain threshold) on monthly-to-multi-year time scales (Chou and Lan, 2012; Qian et al., 2022). However, the wet season process is more interesting to agroclimatological users but less known, as the start and end of wet seasons not only determine crop sowing dates (Zhang et al., 2021a), but also play a critical role in flood and drought prevention (Kniveton et al., 2009; Faradila and Bowo, 2023). Rainfall intensity, frequency, and intra-variability are important features of wet-season processes and climate models (Wang et al., 2014; Liu et al., 2022). The dry spell index (i.e. consecutive dry days) also supplements the extreme fluctuation of a dynamic wet season (Dietzsch et al., 2017). This study attempts to construct a more detailed wet-season regime to provide a comprehensive assessment of rainfall changes in China.

Additionally, the changing wet season regime also affects the wetting and drying patterns, which are crucial to the current effective regulations and future management of water resource systems. A response of "wet regions getting wetter and dry regions getting drier" has been recognised for the physical reason that global mean precipitation increases by 1-3 % per degree rise of surface air temperature (Allen and Ingram, 2002; Held and Soden, 2006; Chou et al., 2009). Hence, a similar conclusion was reached regarding the seasonal cycle change that "wet seasons get wetter and dry seasons get drier" (Chou and Lan, 2012; Chou et al., 2013). However, reports discovered 9.5 % of global land area with a robust "dry gets wetter, wet gets drier" pattern using over 300 combinations of various hydrological data sets from 1948 to 2005 (Greve et al., 2014). These conflicting results may be partly due to the terrestrial paradigm originating from oceanic data (Durack et al., 2012; Roderick et al., 2014). Another potential reason may be hydroclimatological regime shifts with great uncertainties and largely unknown underlying mechanisms related to circulation patterns (Ghassabi et al., 2022; Ma et al., 2022a; Chen et al., 2023), local topography (Cuo and Zhang, 2017; Li et al., 2022c), and energy balance and so on (Kuricheva et al., 2021; Freire et al., 2022; Shiogama et al., 2022). Such topics need to be discussed in China under the current case study, mainly in Africa but with global heterogeneity (Konapala et al., 2020; Palmer et al., 2023).

In this study, we address these issues using an improved method to robustly capture seasonal water cycles in an automated manner (Liebmann et al., 2012). Based on the definition of the cumulative daily rainfall anomaly, we propose a rainfall regime framework (Table 1) to fully uncover the dynamics of the wet season. New daily precipitation data spanning nearly 40 years have been used to characterise wet seasons at the pixel level (Han et al., 2023). This study provides the latest quantitative integration of the wet season and its evolution over the last four decades to refine the existing patterns.

2. Data and methods

2.1. Data

2.1.1. Precipitation data sets

A new daily gridded precipitation dataset for the China mainland (CHM_PRE, as a member of the China Hydro-Meteorology dataset) provides long-term precipitation with spatial resolution of 0.1° from 1961 to present (Han et al., 2023). It overcomes previous limitations by 1) using daily observations from 2839 stations located across China and nearby regions; 2) fully accounting for topographic effect; and 3) balancing local data fidelity and global fitting smoothness in the interpolation of precipitation. Comparisons between the 45 992 high-density gauge observations show the CHM_PRE has the consistent temporal patterns of monthly precipitation series and the best overall performance within the existing gauge-based precipitation in China, including

Table 1Rainfall metrics of wet season regime.

Variables	Definitions	Units
Onset of wet season (onset)	The minimum value in the accumulative anomaly of daily rainfall	Day of year (DOY)
Cessation of wet season (cessation)	The maximum value of the accumulative anomaly of daily rainfall	DOY
Length of wet season (LWS)	Number of days between the onset and cessation of the wet season	Days
Seasonal rainfall amount (R)	Rainfall amount during the wet season	mm
Rainy days (RD)	Number of days with rainfall $\geq 1 \ mm$ between the onset and cessation of the wet season	Days
Rainfall intensity (RI)	Ratio of the total rainfall within the rainy days and number of rainy days	${\rm mm~day}^{-1}$
Rainfall frequency (RF)	Percent of rainy days: the number of rainy days/length of wet season	%
Inter-annual rainfall variability (CV)	Rainfall coefficient of variation	-
Consecutive dry days (CDD)	Maximum number of consecutive days with rainfall <1 mm during wet season	Days
Dry spell	Rainfall <1 mm/day during a period of at least seven consecutive days	-
Number of dry spells	The number of dry spells during rainy season	-
Length of dry spells	Mean length of dry spells	Days

CN05.1 (Wu and Gao, 2013), CMA V2.0 (Zhao et al., 2014), and CGDPA (Shen et al., 2014). Multi-Source Weighted-Ensemble Precipitation (MSWEP) version 2.2 (Beck et al., 2019b) is a reanalyzed gridded dataset at a 3-hourly and 0.1° resolution since 1979. It has provided that are closer real-time estimates by merging gauge, satellite, and reanalysis precipitation estimates to enhance performance in densely gauged regimes (Beck et al., 2020), with overwhelmingly higher accuracy than ERA5-HRES, ERA-Interim, CHIRPS, CHIPS, GCPP, GPCP, and other datasets (Beck et al., 2019a). Precipitation across China from various datasets are compared in Supplementary Fig. 1, which showed generally similar temporal trends. To maximize the duration of the available datasets and optimize the spatio-temporal scales, we averaged the gauge observations (CHM_PRE) and reanalysis precipitation (MSWEP) in this study.

2.1.2. Aridity types

Aridity index (AI) was calculated as the ratio of precipitation to potential evapotranspiration (PET) (Greve et al., 2019). A big Earth Data Platform for Three Poles (https://poles.tpdc.ac.cn/en/data/8b11da09-1a40-4014-bd3d-2b86e6dccad4/) provides PET with a 1 km resolution (Shouzhang, 2022). China was classed into five aridity level (Franklin and Cardy, 2000): (i) hyper-arid (HD, AI < 0.05), (ii) arid (AD, $0.05 \leq AI < 0.2$), (iii) semi-arid (SD, $0.2 \leq AI < 0.5$), (iv) dry sub-humid (SH, $0.5 \leq AI < 0.65$), and (v) humid regions (HM, AI ≥ 0.65) (Fig. 1, Supplementary Fig. 2a).

2.1.3. Hydrometeorological data

Annual temperature (TMP) and data was derived from the big Earth Data Platform for Three Poles (Shouzhang, 2019). The solar radiation (SOLAR) data was derived from the ERA5-Land monthly averaged data produced by the European Centre for Medium-Range Weather Forecasts (ECMWF) (Muñoz-Sabater et al., 2021). We obtained (root-zone) soil moisture (SM) data from the Global Land Evaporation Amsterdam model (Martens et al., 2017), and resampled them to a 0.1° spatial resolution using the nearest-neighbour interpolation (Wei et al., 2019).

2.2. Methodology

2.2.1. Extension of the Liebmann method for China

In this study, the method described by Liebmann et al. for the entire Africa (Dunning et al., 2016) was used to identify wet seasons in China.

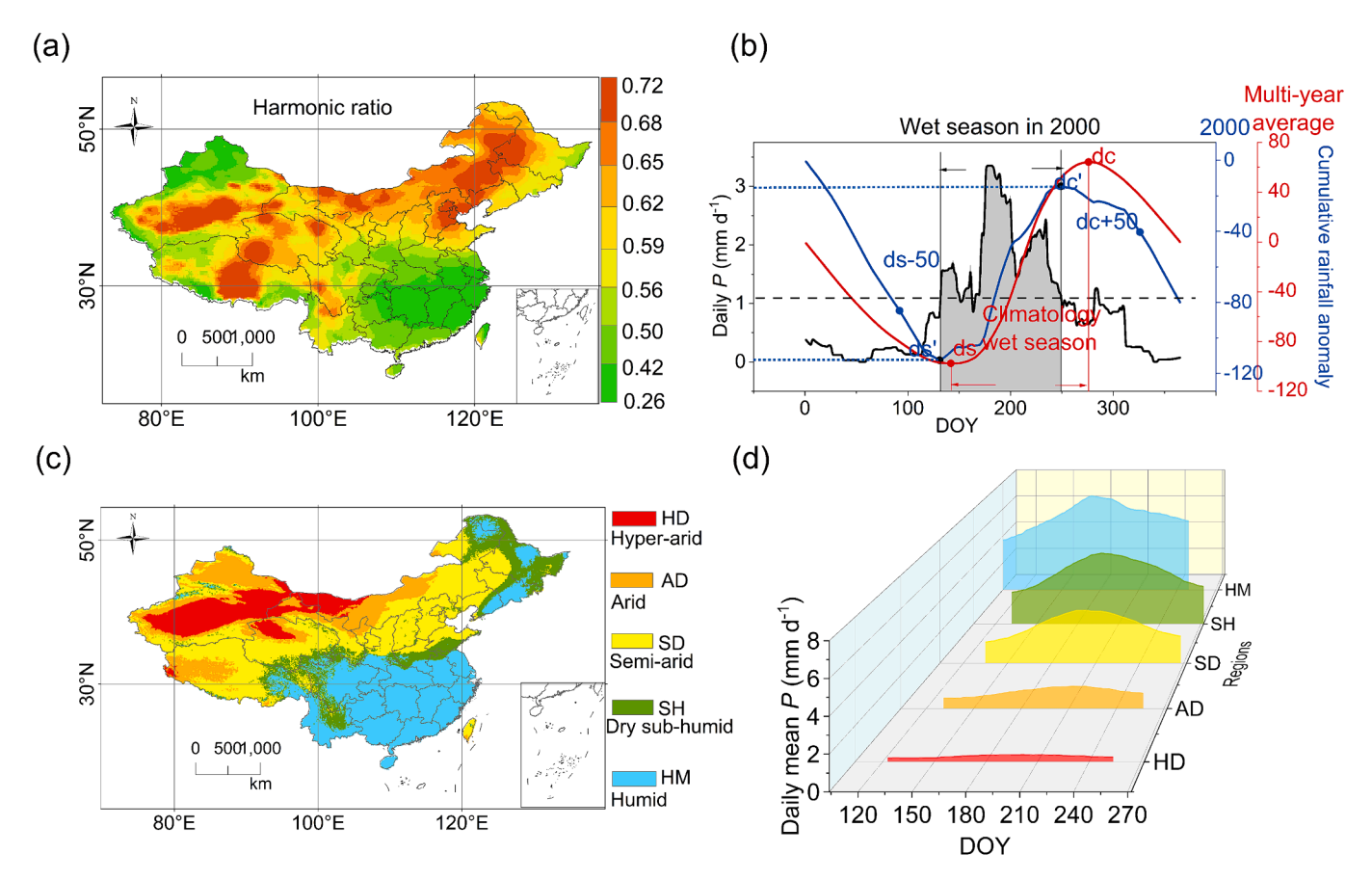


Fig. 1. Seasonality, onset and cessation of the climatological wet season. (a) The ratio of the amplitudes of the second harmonics to the amplitude of the first harmonic per year for each grid point in 1982–2020. (b) Climatological cumulative daily mean rainfall anomaly (red) for 29.8°N, 101.1°E averaged over 1982–2020, cumulative daily mean rainfall anomaly (blue) and daily rainfall (black) in 2000. The gray polygon marks the extent of the wet season in 2000. (c) Spatial distributions of dry and wet regions. HD: hyper-arid; AD: arid; SD: semi-arid; SH: dry sub-humid; HM: humid. (d) Climatological wet season in different regions. DOY represents the day of the year. The Z-axis represents the spatial multiple-year mean daily rainfall. (For interpretation of the references to color in this figure legend, the reader is referred to the web version of this article.)

Rather than setting a unified precipitation threshold, this method calculates cumulative rainfall anomalies in relation to local climatology, which increases when the daily precipitation is above the climatological mean daily rainfall and decreases when the daily precipitation is below the climatological mean daily rainfall (Dunning et al., 2016). The onset and cessation of the wet season correspond to dates with the minima and maxima of cumulative rainfall anomalies (Zhang et al., 2018), respectively, which have mostly been applied to tropical regions, including parts of Western and Central Africa (Sanogo et al., 2015; Froidurot and Diedhiou, 2017), the Sahel (Dunning et al., 2018), and the Intergovernmental Authority on Development (IGAD) regions of eastern Africa (Omay et al., 2023). We adjusted the processes for their application in China, as described in sections 2.2.2-2.2.4. First, harmonic analysis was conducted to determine the number of wet seasons per year (He et al., 2022). Then, using multi-year average time series, we found the "climatological wet season" or the time when wet season typically occurred. Finally, the start and end dates of each wet season were determined for each year.

2.2.2. Estimation of seasonality

Harmonic analysis of time series (HANTS) is a synthesis of smoothing and filtering methods (Gautam et al., 2007), that fully utilises and connects the existing temporal and spatial characteristics of grid data. We performed a Fourier transform on the entire daily time series (Zhou et al., 2022b). The ratio of harmonic amplitudes at frequencies of one and two cycles per year was calculated using HANTS to determine seasonality (Jiang et al., 2019). A ratio less than 1 signifies that a single

wet season fits time series better, otherwise (ratio ≥ 1) the harmonic of two cycles per year is more likely (Dunning et al., 2016). MATLAB was used to conduct the HANTS.

2.2.3. Identification of onset and cessation

The processes for grid points with one wet season cycle are described by Liebmann et al. (2012). For points with two seasonal cycles per year, the dates were determined using the method used for a single season (Dunning et al., 2016). We initially extracted the climatology wet season, which is the period when the wet season occurs, and considered those seasons that span the calendar year (Ferijal et al., 2022), by calculating the climatological cumulative daily rainfall anomaly (C(d)) from the long-term average daily precipitation (R_i^*) in the calendar year. C(d) was calculated using Eq. (1):

$$C(d) = \sum_{i=1,lan}^{d} R_i^* - \overline{R^*}$$
 (1)

In this case, i runs from 1 January to 31 December to calculate the climatological daily mean rainfall \overline{R}^* (displayed by the black line in Fig. 1b); the anomaly is the climatological daily precipitation (R_i^*) minus the daily mean precipitation (\overline{R}^*). Fig. 1b shows C(d) as a red line. In view of this, C(d) increases when R_i^* is greater than \overline{R}^* , and decreases when R_i^* is less than \overline{R}^* , the day with the minimum C(d) marks the start of the wet season (ds), and the day with the maximum C(d) after ds marks the cessation of the wet season (dc).

Subsequently, the start and cessation of the wet season were calculated for each year by applying the individual daily cumulative rainfall

anomalies (C(D)) on a certain day (D) using Eq. (2):

$$C(D) = \sum_{j=ds-50}^{D} R_j - \overline{R^*}$$
 (2)

For individual years, the cumulative rainfall anomaly was calculated for day j, considering the range from ds - 50 to dc + 50. The day with the minimum C(D) marks the start of the wet season (ds') for that year, after which rainfall is consistent in its occurrence and intensity (above R^*). The day with the maximum C(D) after ds' marks the cessation of the wet season (dc') for this year. Fig. 1b shows 2000 as an example of C(D) as the blue line). To reduce synoptic noise, all the precipitation datasets were smoothed beforehand using a 30-day running window. To date, we have a long-term database of the timing of the wet season on a daily scale for each pixel in China.

2.2.4. Regime framework for wet season

Table 1 summarises the rainfall regime metrics used to fully depict the characteristics of wet seasons. Apart from rainfall amount, which is recognised as one of the essential factors of the wet season influencing both primary productivity and human social life, rainfall frequency and rainfall intensity are rising concerns which may benefit woody and herbaceous plants differently (Brandt et al., 2019; Zhang et al., 2019b). These are still one of the complex climate variables used to handle climate monitoring and climate model simulations (Ferijal et al., 2022). The inter- and intra-annual variability of rainfall is affected by climate change and exhibits diverse directions and magnitudes that require further exploration in terms of heterogeneity (Baldocchi et al., 2021). Dry spells were described based on the Global Expert Team on Climate Change and Indices (ETCCDI)-based precipitation climatology (Dietzsch et al., 2017).

2.2.5. Variability analysis

The variance and unranked Gini index (UGI) were used to detect inter-annual and intra-annual variations, respectively (Ritter et al., 2020). The variance was estimated as the standard deviation of the detrended and temporally filtered time series (Schillaci and Schillaci, 2022). The UGI was derived from the economic Gini coefficient, which measures the income disparity among residents. Here, a UGI ranging from 0 to 1 was used to describe the relative degree of irregularity in the daily precipitation distribution. A value of 0 indicates equal rainfall distribution every day, and 1 indicates the concentration of rainfall on the first or last day of the wet season (Ritter et al., 2020). Calculations were performed using R, MATLAB, and ArcGIS.

2.2.6. Trend analysis

Linear regression is widely used to detect significant increasing or decreasing trends in climatic variation based on the least-squares method (Xu et al., 2022). A two-tailed Student's t-test was used to measure the P values of trends (Jiang et al., 2019). The significance level was set at P < 0.05. Trend tests were performed on each rainfall metric at the pixel level using Eq. (3):

$$M_n^y = TM_n \times y + b + \varepsilon \tag{3}$$

where M_n^y is the nth rainfall index in year y. y ranges from 1982 to 2020. TM_n is the regression slope representing the linear rainfall index trend. b is the intercept of the equation, and ε is the error.

For the annual mean precipitation time series, we identified breaks by using the R packages 'segmented', 'tseries', and 'rlang'. The shortest segment was set to 0.25 of the total data length to limit the number of observations in each segment (Hu et al., 2023). The most significant breakpoints were determined using the Chow test (P < 0.05) (Novák and Truong, 2023).

We identified the year 2000 as the breakpoint of the annual mean precipitation time series from multiple datasets (Supplementary Fig. 1). Previous studies identified distinct hydroclimatological variations in China before and after 2000 (Hu et al., 2022). For specific changing amplitudes and statistical comparability, we calculated the changes and changing rates of the rainfall metrics between different periods divided by breaks, using Eq. (4):

$$RM_n = \left(\overline{RM_{np2}} - \overline{RM_{np1}}\right) / \overline{RM_{np1}} \tag{4}$$

where $\overline{RM_{np1}}$ and $\overline{RM_{np2}}$ are the multiple-year mean values of the nth rainfall metric in Table 1 during the first and second periods, respectively, and the difference between them is the change in the nth rainfall metric. RM_n is the rate of change in the nth rainfall metric.

2.2.7. Relative importance evaluation

We used a bootstrap technique based on the method developed by Lindemann, Merenda, and Gold (LMG) to calculate the relative significance of the contributors to changes during the wet season (Liu et al., 2021). Key components of energy and water cycles, including changes in near-surface temperature (TMP), SOLAR, SM, PET, and annual precipitation (PRE), are used to explain the variation in the length of wet season (LWS) from the viewpoint of their contribution to R² (Shi et al., 2021). Before modelling, all variables (V) were normalised for each grid cell (x, y) for each year (t) using the Z-score by Eq. (5):

$$V_{zcore,t(x,y)} = \frac{V_{t(x,y)} - \overline{V_{1982-2020(x,y)}}}{\sigma(V_{1982-2020(x,y)})}$$
(5)

where $\sigma(V_{1982-2020(xy)})$ is the standard deviation, and $\overline{V_{1982-2020(xy)}}$ is the mean of values during 1982–2020. All variables were tested for no multicollinearity by variance inflation factor values (VIF < 5) (Wei et al., 2019). The model was conducted for the drylands, humid areas and the whole China.

3. Results

3.1. The onset and cessation of wet season

The maximum harmonic ratio was less than 0.72 across all regions (see Section 2.2.2), indicating that each grid point experienced a distinct wet season (Fig. 1a). Subsequently, the wet season was diagnosed based on cumulative daily rainfall anomalies (Fig. 1b). Finally, the identified wet seasons and their onsets and cessations are summarised for the five dryland subtypes and humid regions (Fig. 1c). On average, the wet season begins earliest in humid regions on 14 April (Fig. 1d). For the dryland subtypes, the drier the area, the earlier the wet season began and ended (mean on September 30, 26, 13, and 10, respectively). Across China, more humid areas experienced longer wet seasons, averaging 122, 126, 133, 140, and 145 d for humid, dry sub-humid, semi-arid, arid, and hyper-arid areas, respectively.

3.2. Spatial-temporal trends of wet season

To clearly show the long-term changes in the wet season, we compared the differences in the wet season onset, cessation, and length between 1982 and 2000 and 2001–2020 periods. The results showed that the wet season increased in 66.76 % of the drylands (both from the perspective of trends and changing rates, P < 0.05) and in 59.43 % of the humid areas (Fig. 2a, Supplementary Fig. 3, P < 0.05). The reasons for the variations in the duration of the wet season are different. The earlier occurrence in hyper-arid and dry sub-humid areas contributed to prolonged wet season duration by an average increase of 3.24 ± 1.98 and 3.65 ± 0.93 days after 2000 (Fig. 2b, e, P < 0.01). The wet season in arid, semi-arid and dry sub-humid areas prolonged by 14.43 ± 1.54 , 8.28 ± 1.37 days during the past four decades due to both the earlier onset (decreasing purple lines in Fig. 2c, d, P < 0.01) and later cessation (increasing orange lines in Fig. 2 c, d, P < 0.01). Humid areas displayed slightly shortening wet season length with the decreasing trend of P < 0.01

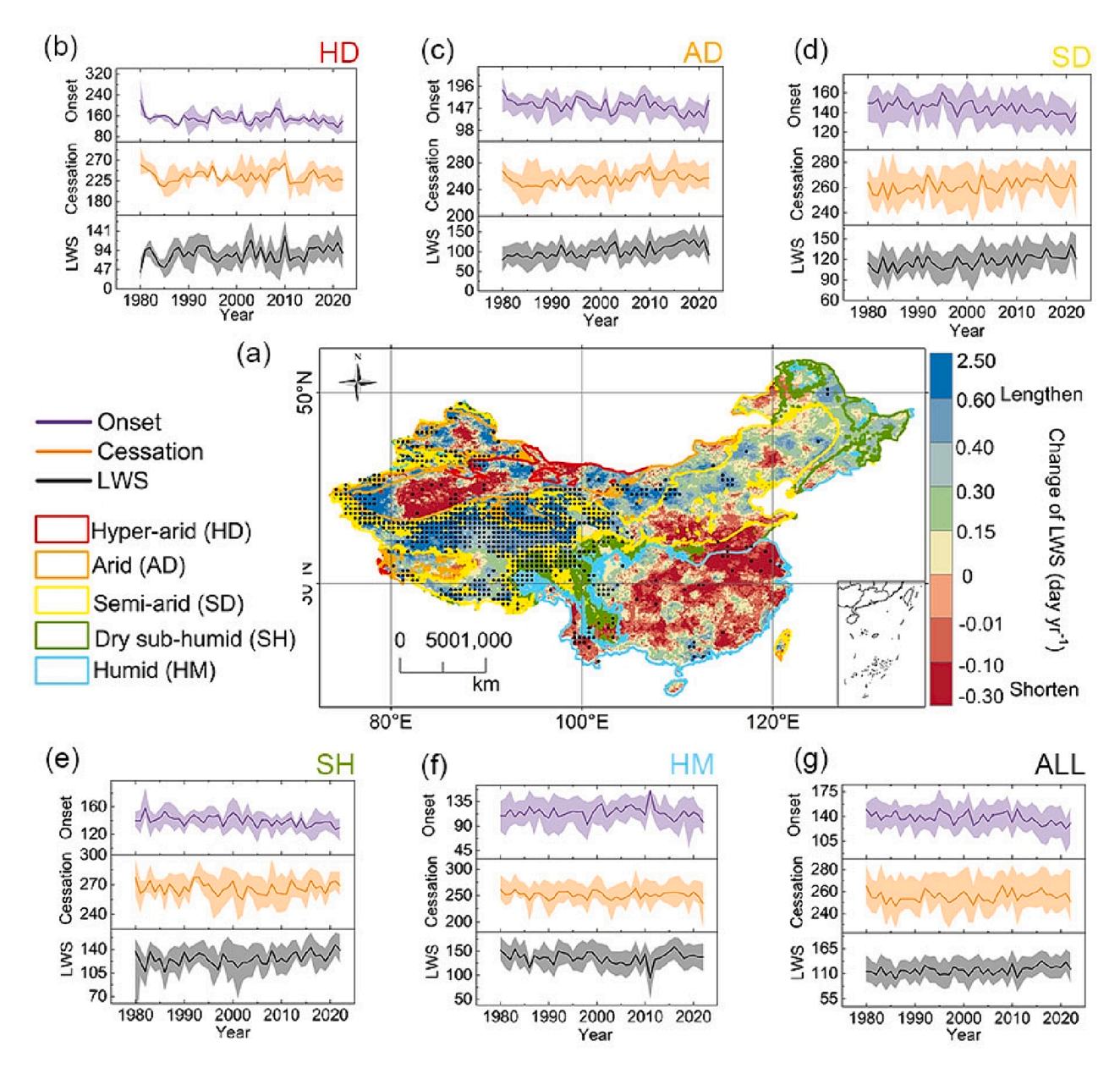


Fig. 2. Spatial patterns of changes in the length of wet season (LWS). (a). Linear trends of LWS. The black dots represent grid points with trends of significance level of P < 0.01. (b)-(g) plot time series of onset (purple), cessation (orange) and duration (black) during 1982–2020 in different dry and humid areas. (For interpretation of the references to color in this figure legend, the reader is referred to the web version of this article.)

 0.15 ± 0.18 (black lines in Fig. 2f, P<0.05), although the whole regions displayed significant increasing length of wet season by 4.44 \pm 1.55 days (Fig. 2g, P<0.01). In general, we found a pattern in China's wet season that "in wet area gets shorter and in dry area gets longer" over the last four decades.

3.3. Inter- and intra-annual variability of rainfall

On an annual timescale, the amount of rainfall during the wet season fluctuated more violently from humid to dry areas (Fig. 3a). The hyperarid and arid areas were characterised by high inter-annual variability (i.e. variance). During the wet season, the majority of regions that experienced uniform rainy days was humid. In addition to the mean state, changes in the inter- and intra-annual rainfall variability were further characterised by asynchronous patterns. Over the last four decades, semi-arid and humid areas have displayed the greatest negative and positive inter-annual variability during the wet season, respectively

(Fig. 3b). However, the intra-annual variability experienced a broad decrease, with a greater decrease in the UGI in less dry areas in dryland subtypes (Fig. 3c). The disagreement in the changing patterns of precipitation variability at different timescales suggests that increased inter-annual variability (i.e. variance) and decreased intra-annual variability (i.e. UGI) help allocate daily rainfall in the wet season, especially in the eastern coastal areas (Supplementary Fig. 6).

3.4. The relationships between rainfall and aridity

The multi-year average of seasonal rainfall amount ranged from 274.83 ± 212.34 mm in the drylands to 801.30 ± 208.96 mm in the humid areas, indicating a highly coherent spatial pattern with rainfall intensity gradually increasing from 2.61 ± 1.43 mm/day (in the drylands) to 6.24 ± 1.54 mm/day (in the humid areas) (Fig. 4, P<0.05). Locations with rainy days of up to four months (120 days) were found in $76.34\,\%$ of the dry sub-humid and humid areas, whereas $78.84\,\%$ of the

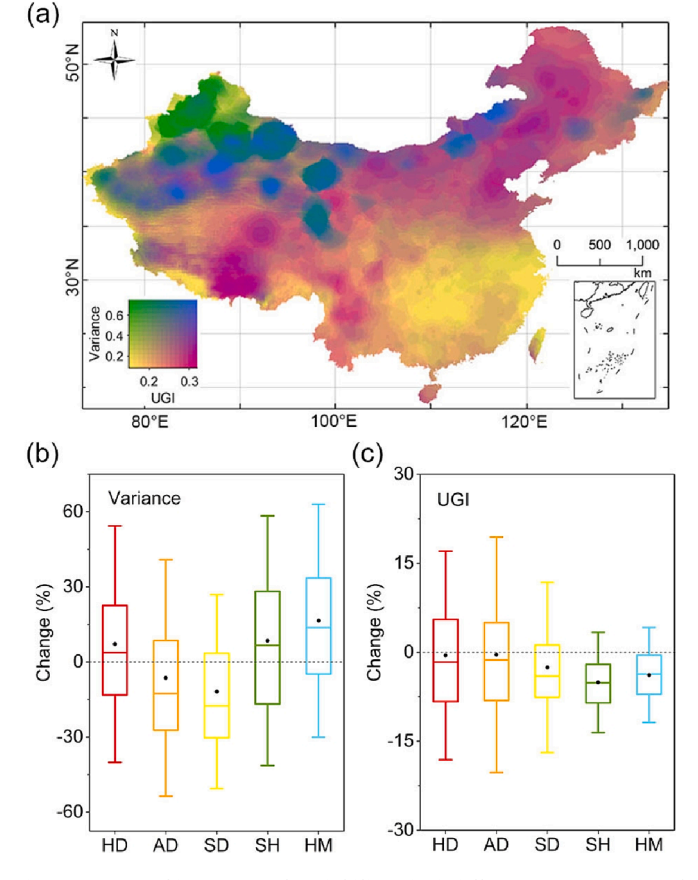


Fig. 3. Inter- and intra-annual variability of rainfall. (a) Mean variance and UGI during 1982–2020. (b) Changing rates in variance from 1982 to 2000 to 2001–2020 for different wet and dry regions shown in Fig. 1c. (c) The same as (b) but for UGI.

hyper-arid and arid areas had less than 60 rainy days. Interestingly, the trends in the rainfall amount, rainy days, and rainfall intensity showed consistent pairwise patterns, contrary to the respective mean states. That is, significantly increasing trends were dominant in areas with less rainfall/rain days/rainfall intensity, such as almost all arid regions, whereas decreasing trends were mostly detected in areas with more abundant rain, such as humid areas. Moreover, temporal changes in rainfall were positively correlated with dryness. The positive magnitude of rainfall amount change in wet season was greatest in arid and semiarid areas, with a rise of 18.51 \pm 20.18 % and 1.41 \pm 0.83 mm/year on average, and lowest in humid areas, with a drop of 7.81 \pm 4.97 % with 2.32 \pm 1.67 mm/year on average (Fig. 4, P < 0.05). Rainy days (i. e., days with rainfall ≥ 1 mm) markedly increased in the arid areas of 3.52 \pm 1.08 days and semi-arid areas of around 6.30 \pm 1.05 days, but decreased in the humid areas of -2.77 ± 0.77 days after 2000 (Supplementary Fig. 6, P < 0.05). There was a greater reduction in rainfall intensity in drylands with lower dryness. The increase in rainfall intensity in parts of humid eastern areas may have been caused by prevailing shortening of the wet season, albeit with less rainfall. Overall, changes in rainfall regimes showed that wet seasons in arid areas became wetter, whereas in wet areas became drier.

To assess the applicability of the increase in precipitation variability that triggers wider swings between wet and dry conditions, we compared dry spell changes. Dry spells generally occurred more frequently and lasted longer in drier areas, with mean lengths ranging from 2.21 \pm 0.37 to 26.14 \pm 13.25 days per dry spell, mean numbers ranging from 0.21 \pm 0.03 to 1.73 \pm 0.54, and mean consecutive dry days from 4.39 \pm 0.44 to 35.21 \pm 18.51 days in dry sub-humid and arid areas, respectively (Fig. 5a-c). Changes in dry spells displayed

heterogeneous spatial patterns in both direction and magnitude; however, all showed a declining line with aridity (Fig. 5d-i). The extended wet seasons in drier regions not only gave rise to the occurrence of rainy days, but also consecutive dry days, with a mean rise of 12.42 ± 11.23 days in 73.47 % in the hyper-arid and arid areas (Fig. 5j-l). Dry spells occurred more frequently in 60.94 % of the arid regions and lasted 0.11 \pm 0.06 more days per dry spell after 2000 (Supplementary Fig. 6). The co-occurrence of positive changes in the direction of rainy and dry days indicates an exacerbated risk of floods and droughts under global warming at the regional scale.

4. Discussion

Using a unified framework and a variety of metrics, we reconstructed the onset and cessation dates of the wet season in China over the last four decades to investigate the potential dynamics of hydrological responses to global warming. The state-of-the-art precipitation datasets allow more accurate application of the Liemann method via accumulated daily precipitation anomalies. Two opposing trends were detected during the advancement of the wet climatological season. One was the first invasion in the central humid areas (on 5 April), and the other was the initial launch in the hyper-arid areas (on 5 May) and downwards to the dry subhumid areas (on 11 May). These results are consistent with the major wet season determined by the threshold of the standardised climatic pentad rainfall records from Chinese stations (Zhan et al., 2016). In drylands, the wet season commences slightly earlier in the northern part than in the southern part, owing to the effects of westerlies with obvious local features (Zhang et al., 2021b). Moreover, the intensity of the Tibetan Plateau Monsoon may help transport cold air from high latitudes southward, prompting precipitation and triggering the wet season in the southwest regions (Zhang et al., 2022). The quantified onset and cessation of wet seasons in a modified manner for each pixel provides a more precise analysis of the local characteristics of wet season processes than previous subjective and semi-objective descriptions across China.

Wet season changes in time and space become more complex and unknown as climate warming and hydrological cycles intensify (Zhang et al., 2018; Brandt et al., 2019; Li et al., 2022b). In contrast to the global "wet gets wetter, dry gets drier" paradigm (Liu and Allan, 2013), this study confirms the paradigm in China that "wet areas get drier, dry areas get wetter" through analysis of various factors such as the length of the wet season, precipitation amount, number of rainy days, and rainfall intensity. Similar patterns of rates and linear trends support these changes. On a temporal scale, the daily precipitation was distributed more uniformly during the wet season in humid areas (Fig. 3). Our findings align with the global re-assessment of land-based wetting and drying trends, emphasising that the catchphrase "DDWW" oversimplifies the complexity of these processes over land (Greve et al., 2014).

Another new revolution of wet season in relation to duration is that "in wet areas gets shorter, in dry areas gets longer" (Fig. 6a). We attributed these annual changes in LWS during 1982-2020 to potential hydrothermal conditions using a relative importance algorithm. Changes in annual precipitation and SM were the leading controlling factors, with relative weights of 54.96 % and 39.03 % in the drylands, and 45.25 % and 34.70 % in humid areas, respectively (Fig. 6b). China is located at the mid-latitudes and is influenced by the subseasonal monsoon system. The East Asian monsoon rain belt migrated northwest from the Last Glacial Maximum to the mid-Holocene, leading to increased precipitation and a longer wet season in northern China (Yang et al., 2015). Disrupted summer winds can reduce rainy days and shorten the length of the wet season in the humid regions of South China (Yao and Wang, 2021). In particular, the dynamic synergy of the Qinghai-Tibetan Plateau summer monsoon and boreal summer intra-seasonal oscillations can lead to changes in drought and flooding during the wet season in southwest China (Li et al., 2022a). In this regard, wet season changes may benefit northern agriculture while posing

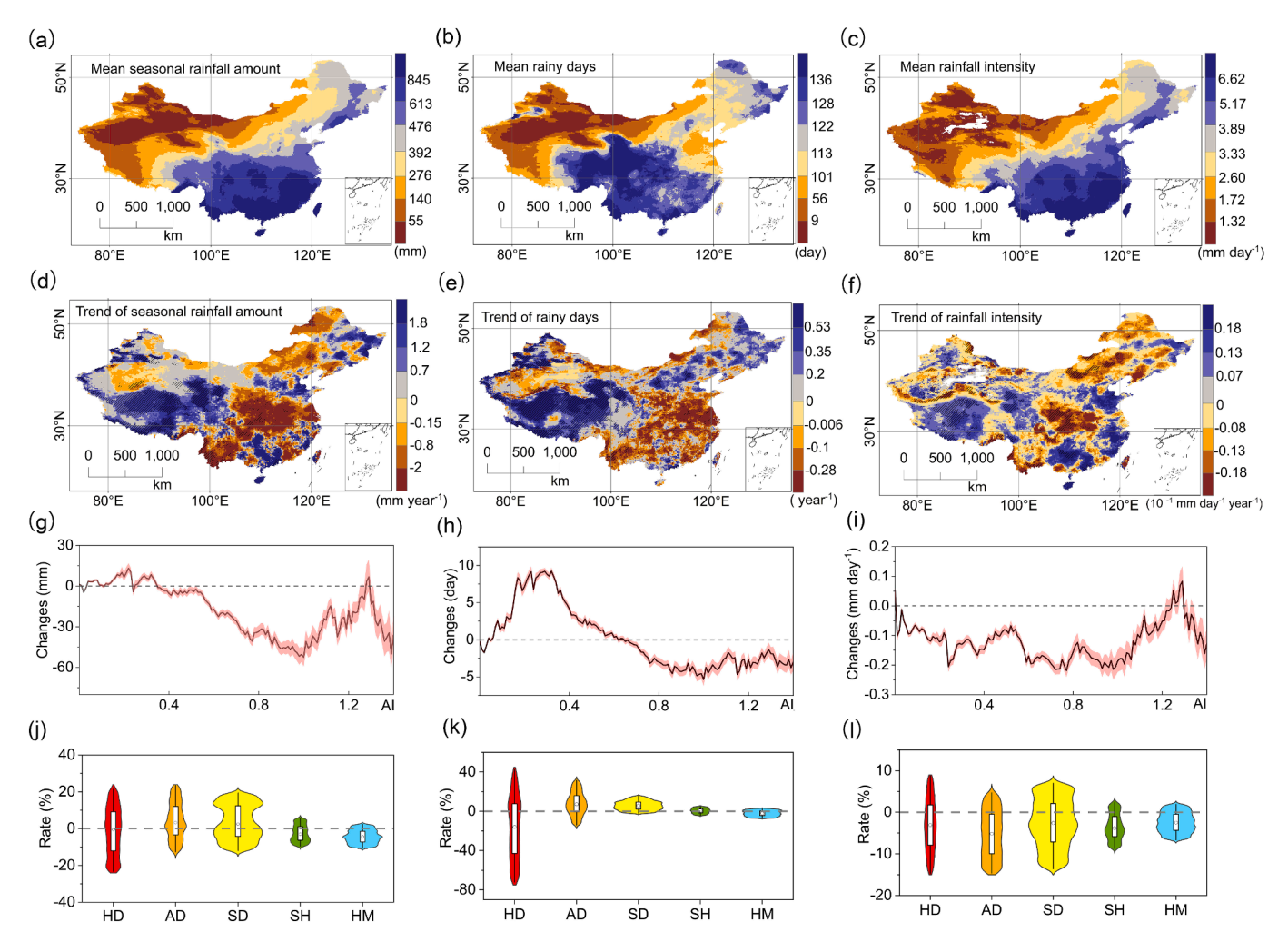


Fig. 4. Changes of rainfall in wet season and response to aridity. (a), (b) and (c) show spatial patterns of mean rainfall amount, rainy days and rainfall intensity, respectively. (d), (e), and (f) show the corresponding trends during past four decades. The areas with black diagonal lines display significant changes in rainfall regimes with P < 0.05. (g), (h) and (i) plot the amplitude of changes along the aridity. (j), (k) and (l) show rates in 2001–2020 on the baseline of 1982–2000. The color of the violin box generates rate values in four dryland subtypes and humid areas, for more categorization details in 2.1.2 Aridity types and Supplementary Fig. 2.

drought risks in the south. For example, the continuously decreasing water level in Poyang Lake, as well as SM around China's largest freshwater lake, has been a serious concern in wet areas (Li et al., 2023). Therefore, it is necessary to examine the evolution of the wet season at different scales to monitor regional risks and promptly adjust for global climate governance.

One large-scale explanation is the interdecadal oscillation of seawater in the North Pacific (Zhang et al., 2021b). The cold phase of the Pacific Decadal Oscillation (PDO) over the last four decades has resulted in increased precipitation in the drylands of China (Jiang et al., 2023). The other underlying physical mechanism is the Clausius-Clapeyron relationship, where moisture increases by 6–7 % for per Kelvin of temperature increase (Neelin et al., 2022). The general trend is that temperatures at higher latitudes climb faster than those at lower latitudes, contributing to a larger increase in moisture during the wet season in drier regions, which also provides a possible principle to predict global dry-wet transitions (Wang et al., 2023).

Simultaneously, we found that variations of dry spells increased as the drought intensified across most of China's drylands. This change represents the nonlinear progression of an increase in dryness severity due to dry spells, as evidenced by the increasing temporal trends and spatial tendencies to expand. For example, the average length of dry spells was extended to 70.89 % of the arid areas (Supplementary Fig. 6). The number of dry spells increased by 71.09 % in arid areas, at an

increase rate of 19.56 %. Interestingly, dry spells revealed that nearly 63.22 % of the area with increasing dryness received more rainfall, indicating that the monsoon wet season shifted toward more frequent extreme rainy and dry spell events (Donat et al., 2016; Huang et al., 2022). Increased rainy days contribute to an increase in the total precipitation, which may mask drought progression through dry spells (Ferijal et al., 2021). Hence, an impression based on accumulated precipitation may lead to a misinterpretation of intermittent drought development, although it may display a wide increase (Yu and Zhai, 2020; Li et al., 2021; Ma et al., 2022b).

In contrast to the threshold-based derivation that covers the entire region, the improved Liebmann statistical analysis considers climatic variability and local responses to maximise guidance for local agricultural arrangements (Dunning et al., 2016). The wet season framework proposed herein is crucial for effective water resource management because it can capture rainfall features with fine spatial resolution. The adaptability of comprehensive wet season estimations allows for rational planning and full utilisation of rainfall over a variety of time periods (Granato-Souza et al., 2020). Furthermore, because rainfall is closely linked to natural disasters such as floods and droughts, our long-term trend analysis at the pixel level is essential for improving local risk assessments and effective strategy formulation. Researchers have suggested drawing cautious conclusions from global to local patterns, owing to the co-occurrence of significantly increasing rain and dry days in drier

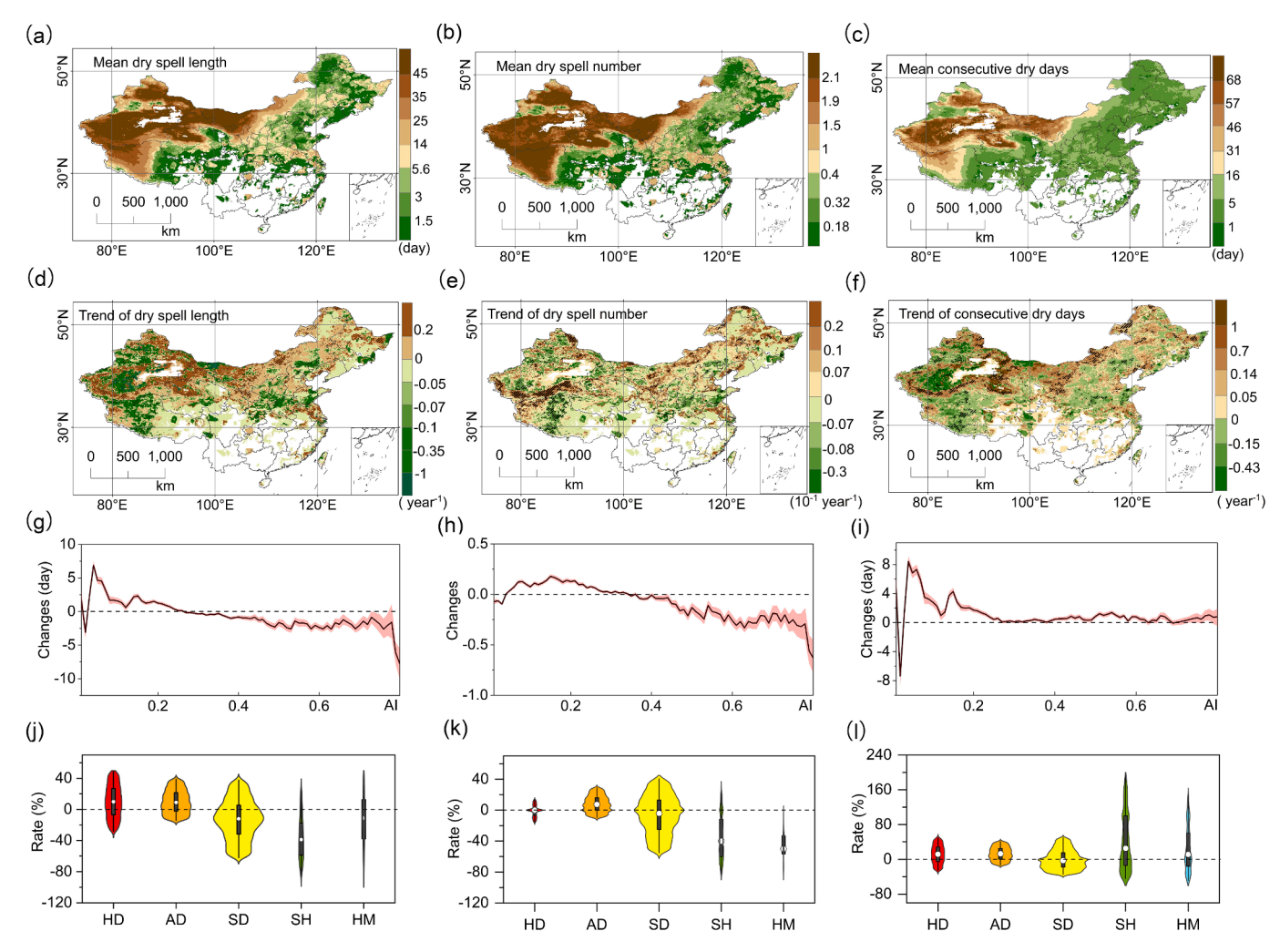


Fig. 5. Changes of dry spells in wet season and response to aridity. (a), (b), and (c) display spatial patterns of dry spell length, dry spell number and consecutive dry days, respectively. (d), (e) and (f) show the corresponding trends. The areas with black diagonal lines display significant changes in rainfall regimes with P < 0.05. (g), (h) and (i) plot the changes along the aridity. (j), (k) and (l) show the changing rates on drylands and humid regions. The color of violin box represents four dryland subtypes and humid areas, for more details in 2.1.2 Aridity types.

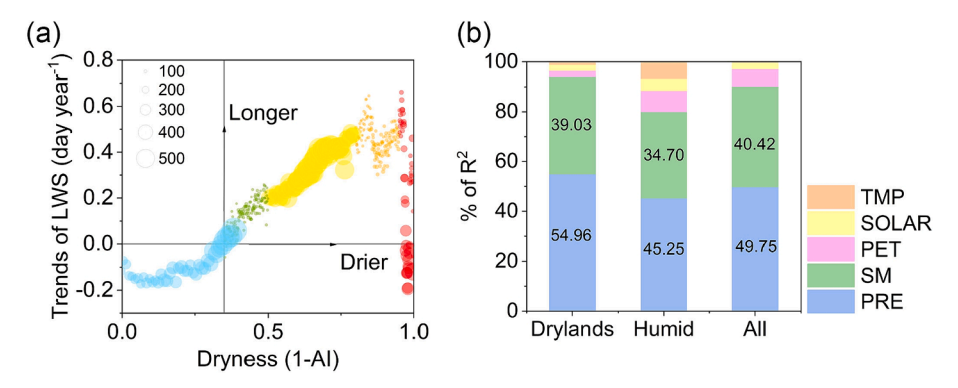


Fig. 6. Trends of length of wet season (LWS) along dryness. (a) The dryness is calculated by 1-AI. The diameter of the bubble is representative of the number of grid cells for integration by mean values. The colours represent the subtypes of dryland classified in 2.1.2. Aridity types and Fig. 1c. (b) Relative importance of controlling factors explaining changes in LWS. Potential variables are changes in precipitation (PRE), soil moisture (SM), potential evapotranspiration (PET), solar radiation (SOLAR), and temperature (TMP).

regions and geographical variability (Chou et al., 2013; Greve et al., 2014; Donat et al., 2016). With the increasing need for climate risk monitoring under global warming, there is an urgent need to develop a globally applicable method to re-evaluate wetting and drying patterns (Zhang et al., 2021b).

5. Conclusion

Through an improved Liebmann statistical approach using daily precipitation records (1982–2020), we quantified the long-term onset and cessation of the wet season and evaluated the rainfall regime

dynamics in China. The wet season duration changed in the opposite direction, becoming shorter in wet regions and longer in dry regions. Rainfall amount and rainy days significantly increased in dry regions (/on drylands) and decreased in wet regions, resulting in the wet season mode of "in wet areas getting drier, in dry areas getting wetter". Moreover, a similar pattern was observed for dry spells, as indicated by a larger increase in dry spell length, number of dry spells, and consecutive dry days with increasing dryness. Concurrent increases in rainy days and dry spells suggest a tendency of rainfall regimes toward more frequent extreme conditions in drier areas. These observed changes emphasise the importance of our comprehensive framework for characterising dynamic rainfall regimes, which serve as the foundation for addressing climate-related risks, optimising water allocation, and boosting agricultural prosperity.

CRediT authorship contribution statement

Ying Hu: Writing - review & editing, Writing - original draft, Visualization, Validation, Methodology, Investigation, Formal analysis, Conceptualization. Fangli Wei: Writing - review & editing, Methodology. Bojie Fu: Supervision, Project administration, Funding acquisition, Conceptualization, Resources. Shuai Wang: Writing - review & editing, Methodology, Investigation. Xiangming Xiao: Writing - review & editing, Visualization, Formal analysis. Yuanwei Qin: Writing - review & editing. Shihua Yin: Writing - review & editing, Methodology, Formal analysis. Zhuangzhuang Wang: Writing - review & editing, Formal analysis. Lingfan Wan: Writing - review & editing, Formal analysis.

Declaration of competing interest

The authors declare that they have no known competing financial interests or personal relationships that could have appeared to influence the work reported in this paper.

Data availability

I have shared the link to my data at the Attach File step

Acknowledgments

This study was supported by the National Natural Science Foundation of China [grant no. 42041007], the Bureau of International Cooperation, Chinese Academy of Sciences [Joint CAS-MPG Research Project, grant no. HZXM20225001MI] and the U.S. National Science Foundation [grant no. 1911955 and grant no. 2200310].

Data availability

The CHM_PRE dataset is available in https://data.tpdc.ac.cn/zh-ha ns/data/e5c335d9-cbb9-48a6-ba35-d67dd614bb8c. The MSWEP dataset is available in https://www.gloh2o.org/mswep/. The PET data can be obtained from https://poles.tpdc.ac.cn/en/data/8b11da09-1a40-4 014-bd3d-2b86e6dccad4/. The temperature and solar radiation data are derived from https://poles.tpdc.ac.cn/en/data/71ab4677-b66c -4fd1-a004-b2a541c4d5bf/ and https://cds.climate.copernicus. eu/cdsapp#!/dataset/reanalysis-era5-land-monthly-means?tab=form, respectively. The (root-zone) soil moisture is available in https://www. gleam.eu/. All the data supporting the findings of this study are included in this article (and any Supplementary Files).

Code availability

All computer codes for the analysis of the data are available from the author on request.

Appendix A. Supplementary data

Supplementary data to this article can be found online at https://doi. org/10.1016/j.jhydrol.2024.131243.

References

- Allen, M.R., Ingram, W.J., 2002. Constraints on future changes in climate and the hydrologic cycle. Nature 419, 224-232.
- Baldocchi, D., Ma, S., Verfaillie, J., 2021. On the inter- and intra-annual variability of ecosystem evapotranspiration and water use efficiency of an oak savanna and annual grassland subjected to booms and busts in rainfall. Glob. Chang. Biol. 27, 359-375.
- Beck, H.E., Pan, M., Roy, T., et al., 2019a. Daily evaluation of 26 precipitation datasets using Stage-IV gauge-radar data for the CONUS. Hydrol. Earth Syst. Sci. 23,
- Beck, H.E., Wood, E.F., Pan, M., et al., 2019b. MSWEP V2 global 3-hourly 0.1° precipitation: methodology and quantitative assessment. Bull. Am. Meteorol. Soc.
- Beck, H.E., Wood, E.F., McVicar, T.R., et al., 2020. Bias correction of global highresolution precipitation climatologies using streamflow observations from 9372 catchments. J. Clim. 33, 1299-1315.
- Brandt, M., Hiernaux, P., Rasmussen, K., et al., 2019. Changes in rainfall distribution promote woody foliage production in the Sahel. Commun. Biol. 2, 133.
- Chen, L., Ford, T.W., Swenson, E., 2023. The role of the circulation patterns in projected changes in spring and summer precipitation extremes in the U.S. Midwest. J. Clim. 36, 1943-1956.
- Chou, C., Lan, C.-W., 2012. Changes in the annual range of precipitation under global warming. J. Clim. 25, 222-235.
- Chou, C., Neelin, J.D., Chen, C.-A., et al., 2009. Evaluating the "rich-get-richer" mechanism in tropical precipitation change under global warming. J. Clim. 22, 1982-2005.
- Chou, C., Chiang, J.C.H., Lan, C.-W., et al., 2013. Increase in the range between wet and dry season precipitation. Nat. Geosci. 6, 263-267.
- Cuo, L., Zhang, Y., 2017. Spatial patterns of wet season precipitation vertical gradients on the Tibetan Plateau and the surroundings, Sci. Rep. 7, 5057.
- Dai, L., Cheng, T.F., Lu, M., 2020. Summer monsoon rainfall patterns and predictability over Southeast China, Water Resour, Res. 56.
- Dietzsch, F., Andersson, A., Ziese, M., et al., 2017. A global ETCCDI-based precipitation climatology from satellite and rain gauge measurements. Climate 5.
 Donat, M.G., Lowry, A.L., Alexander, L.V., et al., 2016. More extreme precipitation in the
- world's dry and wet regions. Nat. Clim. Chang. 6, 508-513.
- Dunning, C.M., Black, E.C.L., Allan, R.P., 2016. The onset and cessation of seasonal rainfall over Africa. J. Geophys. Res. Atmos. 121, 11405-11424.
- Dunning, C.M., Black, E., Allan, R.P., 2018. Later wet seasons with more intense rainfall over Africa under future climate change. J. Clim. 31, 9719-9738.
- Durack, P.J., Wijffels, S.E., Matear, R.J., 2012. Ocean salinities reveal strong global water cycle intensification during 1950 to 2000. Science 336, 455-458.
- Faradila, R., Bowo, C., 2023. Length of the wet seasons and its effect on food crop productivity (rice, corn, and soybean). AIP Conf. Proc. 2583, 020016.
- Ferijal, T., Batelaan, O., Shanafield, M., 2021. Spatial and temporal variation in rainy season droughts in the Indonesian Maritime Continent. J. Hydrol. 603, 126999.
- Ferijal, T., Batelaan, O., Shanafield, M., et al., 2022. Determination of rainy season onset and cessation based on a flexible driest period. Theor. Appl. Climatol. 148, 91-104.
- Franklin, W., Cardy, G., 2000. The United Nations data bases on desertification. In: Desertification, R. (Ed.), Arnalds O and Archer S. Springer, Netherlands, Dordrecht, pp. 131-141.
- Freire, A.S.C., Vitorino, M.I., de Souza, A.M.L., et al., 2022. Analysis of the energy balance and CO2 flow under the influence of the seasonality of climatic elements in a mangrove ecosystem in Eastern Amazon. Int. J. Biometeorol. 66, 647-659.
- Froidurot, S., Diedhiou, A., 2017. Characteristics of wet and dry spells in the West African monsoon system. Atmos. Sci. Lett. 18, 125-131.
- Funk, C., Harrison, L., Alexander, L., et al., 2019. Exploring trends in wet-season precipitation and drought indices in wet, humid and dry regions. Environ. Res. Lett. 14, 115002.
- Gautam, R.S., Singh, D., Mittal, A., et al., 2007. Harmonic analysis of time-series NOAA/ AVHRR images for hotspot detection and land features classification. IEEE Int. Geosci. Remote Sens. Sympos. 2007, 2971-2974.
- Ge, Q., Guo, X., Zheng, J., et al., 2008. Meiyu in the middle and lower reaches of the Yangtze River since 1736. Chin. Sci. Bull. 53, 107-114.
- Ghassabi, Z., Fattahi, E., Habibi, M., 2022. Daily atmospheric circulation patterns and their influence on dry/wet events in Iran. Atmosphere 13.
- Granato-Souza, D., Stahle, D.W., Torbenson, M.C.A., et al., 2020. Multidecadal changes in wet season precipitation totals over the Eastern Amazon. Geophys. Res. Lett. 47. Greve, P., Orlowsky, B., Mueller, B., et al., 2014. Global assessment of trends in wetting
- and drying over land. Nat. Geosci. 7, 716-721. Greve, P., Roderick, M.L., Ukkola, A.M., et al., 2019. The aridity Index under global
- warming. Environ. Res. Lett. 14, 124006. Guo, J., Hu, S., Guan, Y., 2022. Regime shifts of the wet and dry seasons in the tropics under global warming. Environ. Res. Lett. 17, 104028.
- Guo, B., Zhang, J., Meng, X., et al., 2020. Long-term spatio-temporal precipitation variations in China with precipitation surface interpolated by ANUSPLIN. Sci. Rep.
- Han, J., Miao, C., Gou, J., et al., 2023. A new daily gridded precipitation dataset for the Chinese mainland based on gauge observations. Earth Syst. Sci. Data 15, 3147-3161.

- He, B., Chen, C., Lin, S., et al., 2022. Worldwide impacts of atmospheric vapor pressure deficit on the interannual variability of terrestrial carbon sinks. Natl. Sci. Rev. 9, nwab150.
- Held, I.M., Soden, B.J., 2006. Robust responses of the hydrological cycle to global warming. J. Clim. 19, 5686–5699.
- Hu, Y., Wei, F., Fu, B., et al., 2022. Multifaceted characteristics of aridity changes and causal mechanisms in Chinese drylands. Prog. Phys. Geogr.: Earth Environ. 47, 438–453.
- Hu, Y., Wei, F., Fu, B., et al., 2023. Changes and influencing factors of ecosystem resilience in China. Environ. Res. Lett. 18, 094012.
- Huang, L., Du, H., Dang, Y., et al., 2022. More frequent consecutive extreme precipitation in the dry regions of China. Int. J. Climatol. 42, 9583–9594.
- Jiang, N., Yan, Q., Xu, Z., et al., 2023. Divergent response of eastern China precipitation to the Pacific decadal oscillation during the last Interglacial. Quat. Sci. Rev. 319, 108344
- Jiang, Y., Zhou, L., Tucker, C.J., et al., 2019. Widespread increase of boreal summer dry season length over the Congo rainforest. Nat. Clim. Chang. 9, 617–622.
- Kniveton, D.R., Layberry, R., Williams, C.J.R., et al., 2009. Trends in the start of the wet season over Africa. Int. J. Climatol. 29, 1216–1225.
- Konapala, G., Mishra, A.K., Wada, Y., et al., 2020. Climate change will affect global water availability through compounding changes in seasonal precipitation and evaporation. Nat. Commun. 11, 3044.
- Kuricheva, O.A., Avilov, V.K., Dinh, D.B., et al., 2021. Seasonality of energy and water fluxes in a tropical moist forest in Vietnam. Agric. For. Meteorol. 298–299, 108268.
- Li, J., Bevacqua, E., Chen, C., et al., 2022b. Regional asymmetry in the response of global vegetation growth to springtime compound climate events. Commun. Earth Environ. 3, 123.
- Li, G., Chen, H., Xu, M., et al., 2022a. Impacts of topographic complexity on modeling moisture transport and precipitation over the Tibetan Plateau in summer. Adv. Atmos. Sci. 39, 1151–1166.
- Li, C., Fu, B., Wang, S., et al., 2021. Drivers and impacts of changes in China's drylands. Nat. Rev. Earth Environ. 2, 858–873.
- Li, X.-j., Liu, X., Zhang, H.-y., et al., 2022c. Latitudinal patterns of climatic variables and influence of local topography on climatic variables in the dry valleys of southwestern China. J. Mt. Sci. 19, 1348–1356.
- Li, B., Yang, G., Wan, R., 2023. Reassessment of the declines in the largest freshwater lake in China (Poyang Lake): Uneven trends, risks and underlying causes. J. Environ. Manage. 342, 118157.
- Liebmann, B., Bladé, I., Kiladis, G.N., et al., 2012. Seasonality of African precipitation from 1996 to 2009. J. Clim. 25, 4304–4322.
- Liu, C., Allan, R.P., 2013. Observed and simulated precipitation responses in wet and dry regions 1850–2100. Environ. Res. Lett. 8, 034002.
- Liu, M., Hu, S., Ge, Y., et al., 2021. Using multiple linear regression and random forests to identify spatial poverty determinants in rural China. Spatial Statistics 42. 100461.
- Liu, F., Ouyang, Y., Wang, B., et al., 2020. Seasonal evolution of the intraseasonal variability of China summer precipitation. Clim. Dyn. 54, 4641–4655.
- Liu, F., Wang, B., Ouyang, Y., et al., 2022. Intraseasonal variability of global land monsoon precipitation and its recent trend. NPJ Clim. Atmos. Sci. 5, 30.
- Ma, Z., Sun, P., Zhang, Q., et al., 2022b. The characteristics and evaluation of future droughts across China through the CMIP6 multi-model ensemble. Remote Sens. 14.
- Ma, F., Yuan, X., Li, H., 2022a. Characteristics and circulation patterns for wet and dry compound day-night heat waves in mid-eastern China. Global Planet. Change 213, 103839
- Martens, B., Miralles, D.G., Lievens, H., et al., 2017. GLEAM v3: satellite-based land evaporation and root-zone soil moisture. Geosci. Model Dev. 10, 1903–1925.
- Muñoz-Sabater, J., Dutra, E., Agustí-Panareda, A., et al., 2021. ERA5-Land: a state-of-theart global reanalysis dataset for land applications. Earth Syst. Sci. Data 13, 4349–4383
- Neelin, J.D., Martinez-Villalobos, C., Stechmann, S.N., et al., 2022. Precipitation Extremes and Water Vapor. Curr. Clim. Change Rep. 8, 17–33.
- Novák, V., Truong, T.T., 2023. A combination of fuzzy techniques and chow test to detect structural breaks in time series. Axioms 12.
- Omay, P.O., Muthama, N.J., Oludhe, C., et al., 2023. Observed changes in wet days and dry spells over the IGAD region of eastern Africa. Sci. Rep. 13, 16894.
- Palmer, P.I., Wainwright, C.M., Dong, B., et al., 2023. Drivers and impacts of Eastern African rainfall variability. Nat. Rev. Earth Environ. 4, 254–270.
- Qian, Z., Wang, L., Chen, X., et al., 2022. Heteroscedastic characteristics of precipitation with climate changes in China. Atmosphere 13.
- Ritter, F., Berkelhammer, M., Garcia, C., 2020. Distinct response of gross primary productivity in five terrestrial biomes to precipitation variability. Commun. Earth Environ. 1, 34.

- Roderick, M.L., Sun, F., Lim, W.H., et al., 2014. A general framework for understanding the response of the water cycle to global warming over land and ocean. Hydrol. Earth Syst. Sci. 18, 1575–1589.
- Sanogo, S., Fink, A.H., Omotosho, J.A., et al., 2015. Spatio-temporal characteristics of the recent rainfall recovery in West Africa. Int. J. Climatol. 35, 4589–4605.
- Schillaci, M.A., Schillaci, M.E., 2022. Estimating the population variance, standard deviation, and coefficient of variation: Sample size and accuracy. J. Hum. Evol. 171, 103230.
- Seregina, L.S., Fink, A.H., van der Linden, R., et al., 2019. A new and flexible rainy season definition: Validation for the Greater Horn of Africa and application to rainfall trends. Int. J. Climatol. 39, 989–1012.
- Shen, Y., Zhao, P., Pan, Y., et al., 2014. A high spatiotemporal gauge-satellite merged precipitation analysis over China. J. Geophys. Res. Atmos. 119, 3063–3075.
- Shi, P., Chen, Y., Zhang, G., et al., 2021. Factors contributing to spatial-temporal variations of observed oxygen concentration over the Qinghai-Tibetan Plateau. Sci. Rep. 11, 17338.
- Shiogama, H., Watanabe, M., Kim, H., et al., 2022. Emergent constraints on future precipitation changes. Nature 602, 612–616.
- Shouzhang, P., 2019. 1-km monthly mean temperature dataset for china (1901-2021). A Big Earth Data Platform for Three Poles.
- Shouzhang, P., 2022. 1 km monthly potential evapotranspiration dataset in China (1990-2021). A Big Earth Data Platform for Three Poles.
- Wang, X., Huang, G., Liu, J., 2014. Projected increases in intensity and frequency of rainfall extremes through a regional climate modeling approach. J. Geophys. Res. Atmos. 119, 13271–13286.
- Wang, X., Dettman, D.L., Wang, M., et al., 2020. Seasonal wet-dry variability of the Asian monsoon since the middle Pleistocene. Quat. Sci. Rev. 247, 106568.
- Wang, T., Yin, S., Hua, W., et al., 2023. Decadal variability of extreme high temperature in mid- and high-latitude Asia and its associated North Atlantic air–sea interaction. Clim. Dyn. 61, 4587–4601.
- Wei, F., Wang, S., Fu, B., et al., 2019. African dryland ecosystem changes controlled by soil water. Land Degrad. Dev. 30, 1564–1573.
- Wu, J., Gao, X., 2013. A gridded daily observation dataset over China region and comparison with the other datasets (in Chinese). Chinese J. Geophys. 56, 11021111.
- Wu, C., Li, Q., Dong, L., et al., 2024. Rainy season onset date in Southwest China and the related atmospheric circulations. Atmos. Res. 298, 107127.
- Xu, H., Lian, X., Slette, I.J., et al., 2022. Rising ecosystem water demand exacerbates the lengthening of tropical dry seasons. Nat. Commun. 13, 4093.
- Yang, S., Ding, Z., Li, Y., et al., 2015. Warming-induced northwestward migration of the East Asian monsoon rain belt from the Last Glacial Maximum to the mid-Holocene. Proc. Natl. Acad. Sci. 112, 13178–13183.
- Yao, Y., Wang, C., 2021. Variations in Summer Marine Heatwaves in the South China Sea. J. Geophys. Res.: Oceans 126, e2021JC017792.
- Yu, R., Zhai, P., 2020. More frequent and widespread persistent compound drought and heat event observed in China. Sci. Rep. 10, 14576.
- Zhan, Y., Ren, G., Ren, Y., 2016. Start and End Dates of Rainy Season and their Temporal Change in Recent Decades over East Asia. J. Meteorol. Soc. Jpn. Ser. II 94, 41–53.
- Zhang, M., Abrahao, G., Thompson, S., 2021a. Sensitivity of soybean planting date to wet season onset in Mato Grosso, Brazil, and implications under climate change. Clim. Change 168, 15.
- Zhang, W., Brandt, M., Tong, X., et al., 2018. Impacts of the seasonal distribution of rainfall on vegetation productivity across the Sahel. Biogeosciences 15, 319–330.
- Zhang, W., Brandt, M., Penuelas, J., et al., 2019b. Ecosystem structural changes controlled by altered rainfall climatology in tropical savannas. Nat. Commun. 10, 671.
- Zhang, W., Furtado, K., Wu, P., et al., 2021b. Increasing precipitation variability on daily-to-multiyear time scales in a warmer world. Sci. Adv. 7, eabf8021.
- Zhang, S., Meng, L., Zhao, Y., et al., 2022. The Influence of the Tibetan Plateau Monsoon on Summer Precipitation in Central Asia. Front. Earth Sci. 10.
- Zhang, W., Schurgers, G., Peñuelas, J., et al., 2023. Recent decrease of the impact of tropical temperature on the carbon cycle linked to increased precipitation. Nat. Commun. 14, 965.
- Zhang, C., Wang, Z., Zhou, B., et al., 2019a. Trends in autumn rain of West China from 1961 to 2014. Theor. Appl. Climatol. 135, 533–544.
- Zhao, Y., Zhu, J., Xu, Y., 2014. Establishment and assessment of the grid precipitation datasets in China for recent 50 years (in Chinese). J. Meteorol. Sci. 34, 414–420.
- Zhou, J., Zhang, J., Lambers, H., et al., 2022a. Intensified rainfall in the wet season alters the microbial contribution to soil carbon storage. Plant Soil 476, 337–351.
- Zhou, Q., Zhu, Z., Xian, G., et al., 2022b. A novel regression method for harmonic analysis of time series. ISPRS J. Photogramm. Remote Sens. 185, 48–61.